Hindawi
Journal of Nanomaterials
Volume 2019, Article ID 7152690, 6 pages
https://doi.org/10.1155/2019/7152690

Research Article

Efficient Color Tuning of Upconversion Luminescence from Core-Shell Oxysulfide Nanoparticles

Ying Tian, Jianxin Jiao, Xin Feng, Mingming Xing, Yong Peng, and Xixian Luo

School of Science, Dalian Maritime University, Dalian, Liaoning, 116026, PR., China

Correspondence should be addressed to Mingming Xing; mingmingxing@dlmu.edu.cn and Xixian Luo; luoxx@dlmu.edu.cn

Received 11 March 2019; Accepted 10 April 2019; Published 7 October 2019

Academic Editor: William Yu

Copyright © 2019 Ying Tian et al. This is an open access article distributed under the Creative Commons Attribution License, which permits unrestricted use, distribution, and reproduction in any medium, provided the original work is properly cited.

The $Y_2O_2S:Er^{3+}@Y_2O_2S:Yb^{3+},Ho^{3+}$ core-shell up-conversion (UC) nanoparticles were successfully synthesized by the homogeneous co-precipitation method. The $Y_2O_2S:Er^{3+}@Y_2O_2S:Yb^{3+},Ho^{3+}$ core-shell nanoparticles exhibit bright green emissions under 980 nm excitation, while the triple-ion doped $Y_2O_2S:Er^{3+},Yb^{3+},Ho^{3+}$ sample presents mainly red emissions. The intensity ratio of green-to-red emission of the core-shell and conventional triple-ion doped samples are 2.8 and 0.3, respectively. Investigations on the UC mechanisms show that emissions from Er^{3+} and Ho^{3+} ions are achieved simultaneously in the core-shell nanoparticles. This is due to the efficient energy transfers of $Yb^{3+}\rightarrow Ho^{3+}$ within the shell layer and $Yb^{3+}\rightarrow Er^{3+}$ between the shell and the core. While the triple-ion doped $Y_2O_2S:Er^{3+},Yb^{3+},Ho^{3+}$ sample exhibits mainly the emissions of Er^{3+} along with weak luminescence of Ho^{3+} ion. Since the cross relaxation between Er^{3+} and Ho^{3+} ions in the $Y_2O_2S:Er^{3+},Yb^{3+},Ho^{3+}$ nanoparticles can effectively suppress the emissions of Ho^{3+} ions. Yet, in the core-shell structure, this cross relaxation can be successfully restrained in the core-shell structure where Er^{3+} is in the core and Ho^{3+} is in the shell. Therefore, the construction of core-shell structure can improve the luminescence efficiency and provide a route for adjustment of emission color.

1. Introduction

Upconversion luminescence (UCL) materials with unique luminescent properties have become the research focus due to their promising applications in anti-counterfeiting, solar cells, three-dimensional display and solid-state lasers [1–3]. Rare earth oxysulfide (RE_2O_2S (RE = rare earth)) is an ideal optical functional material [4–11] due to their excellent thermal and chemical stability. In addition, RE_2O_2S materials possess low phonon energy, which is important for efficient UCL [12–16]. It has been reported that the UCL efficiency of RE_2O_2S is comparable to that of β-$NaYF_4$ at excitation of 980 nm [12–14]. Meijerink et al. have shown that the UC internal quantum efficiency of $Gd_2O_2S:Er^{3+}$ is higher than that of β-$NaYF_4:Er^{3+}$ under 1550 nm excitation [15]. Therefore, rare earth oxysulfide is an ideal UC host material holding various promising properties. Furthermore, it is known that the efficiency of UCL is lower than that of conventional luminescence due to its intrinsic luminescence processes, and the tuning of emission color is very limited [16]. Recently, it has been proven that the core-shell structure can effectively improve the properties of UCL and the intensive researches focus on the fluoride material [17, 18]. There are only a few reports about the core-shell structures constructed based on the host material of oxysulfide [19, 20].

In this work, we have successfully synthesized the core-shell nanoparticles (NPs) of $Y_2O_2S:Er^{3+}@Y_2O_2S:Yb^{3+},Ho^{3+}$ by using homogeneous co-precipitation method combined with the solid-gas sulfidation route. The UCL properties of $Y_2O_2S:Er^{3+}@Y_2O_2S:Yb^{3+},Ho^{3+}$ and triple-ion doped $Y_2O_2S:Er^{3+},Yb^{3+},Ho^{3+}$ samples were investigated under excitation of 980 nm laser. We found that the core-shell $Y_2O_2S:Er^{3+}@Y_2O_2S:Yb^{3+},Ho^{3+}$ exhibits bright green emission, while $Y_2O_2S:Er^{3+},Yb^{3+},Ho^{3+}$ presents red emission due to the new channels of energy transfers in the core-shell structure. Further, the cross relaxation between Er^{3+}

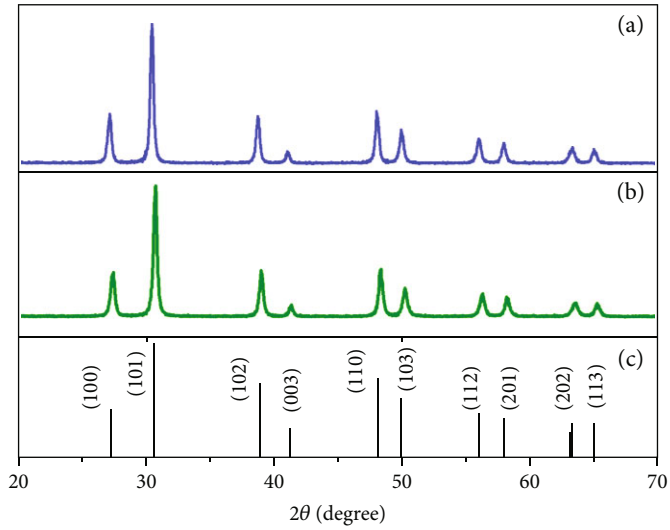

Figure 1: XRD spectra of (a) Y_2O_2S: Er^{3+}, (b) Y_2O_2S: Er^{3+}@Y_2O_2S: Yb^{3+}, Ho^{3+} nanocrystals and (c) standard card of hexagonal Y_2O_2S (JCPDS: No.24-1424).

and Ho^{3+} ions can be successfully restrained in the core-shell structure, which lead to the emissions from both of the Er^{3+} and Ho^{3+} ions. Therefore, the core-shell structure provides a new route for adjustment of luminescence color and improvement of luminescence efficiency.

2. Material and Methods

2.1. Synthesis of the Core-Shell NPs. The precipitates of the core material, $Y(OH)CO_3$:12% Er^{3+}, were obtained by mixing the solution of urea (99% purchased from Tianjin Bodi Chemical Co., Ltd) in 0.8 L solution (7.5 mol/L) and rare earth nitrates $Re(NO_3)_3$ (99.99%, Guangzhou Rare Earth Industry Group CO., Ltd) in 0.2 L solution. The mole ratio of Y, Er ions is 88 : 12. After the centrifuging and washing with water and isopropanol, the core material of Y_2O_3:Er^{3+} powder was achieved by annealing the precipitates at 600°C for 1 h. To coat the shell layer on the core material, we first added the Y_2O_3:Er^{3+} into the urea solution (6 mol, 0.8 L) at 60°C, and then mixed the solution (0.2 L) of $Re(NO_3)_3$ (Re = Y, Yb, Ho, with mole ratio of 91 : 8 : 1) by bath sonication at 80°C for 30 mins. After the similar processes of cooling down, centrifuging, washing and drying, we obtained the precursor of Y_2O_3:Er^{3+}@-$Y(OH)CO_3$:Yb^{3+}, Ho^{3+}. The precursor of the reference sample, $Y(OH)CO_3$:12% Er^{3+},8%Yb^{3+},1%Ho^{3+}, were obtained in the similar processes by mixing the solution of urea with $Re(NO_3)_3$ (Re = Y, Er, Yb, Ho with mole ratio of 79 : 12 : 8 : 1). Then, the core-shell NPs of Y_2O_3: 12%Er^{3+}@Y_2O_3:8%Yb^{3+} and Y_2O_3:Er^{3+},Yb^{3+},Ho^{3+} were finally achieved by annealing the precursor at 600°C. The last step is the sulfidation process. The oxides and sulfur powders were put into a quartz tube which was heated up to 800°C for 30 mins. In this process, Argon was used as protection atmosphere. The above RE-ions doping concentrations were optimized on basis of a series of experimental results as shown in the supporting information.

2.2. Characterization. X-ray diffraction (XRD) patterns were recorded at 40 kV and 40 mA by using a Rigaku D/MAX-Ultima X-ray diffractometer with Cu K α (λ = 0.15406 nm) radiation. The UC luminescence spectra were measured by using the Hitachi F-4500 spectrometer equipped with a 980 nm laser diode (with power density of 0.15w/mm^2). The slit width is 2.5 nm and the scanning speed is 2400 nm/min. The morphology and size of NPs was characterized by using a JEM-2000EX transmission electron microscope (TEM).

3. Results and Discussion

Figure 1 (a) and (b) show the XRD patterns of Y_2O_2S:Er^{3+} and Y_2O_2S:Er^{3+}@Y_2O_2S:Yb^{3+},Ho^{3+} samples. It can be observed that all the diffraction peaks can be indexed to the hexagonal Y_2O_2S compared with the standard card (JCPDS: No.24-1424) in Figure 1 (c). According to the Scherrer formula,

$$D = \frac{0.89\lambda}{(BCos\theta)} \quad (1)$$

where D is the mean crystalline size, λ is the X-ray wavelength, B is the full width at half maximum (FWHM), and θ is the diffraction angle, the calculated crystalline size of Y_2O_2S:Er^{3+} and Y_2O_2S:Er^{3+}@Y_2O_2S:Yb^{3+}, Ho^{3+} are 27.5 and 38.8 nm, respectively. The increase of the nanocrystalline size after the shell coating indicates the formation of core-shell structure which have the same matrix compositions in the core and shell layers [21, 22].

The size and morphology of the samples are studied by TEM measurements, as shown in Figure 2. The precipitates of the core material ($Y(OH)CO_3$:Er^{3+}) are dispersed spherical nanoparticles with a mean particle size about 41 nm (Figure 2(a)). After annealing the $Y(OH)CO_3$:Er^{3+} sample at 600°C and further coated with the shell of $Y(OH)CO_3$:Yb^{3+}, Ho^{3+}, the precipitates of Y_2O_3:Er^3 +@$Y(OH)CO_3$:Yb^{3+},

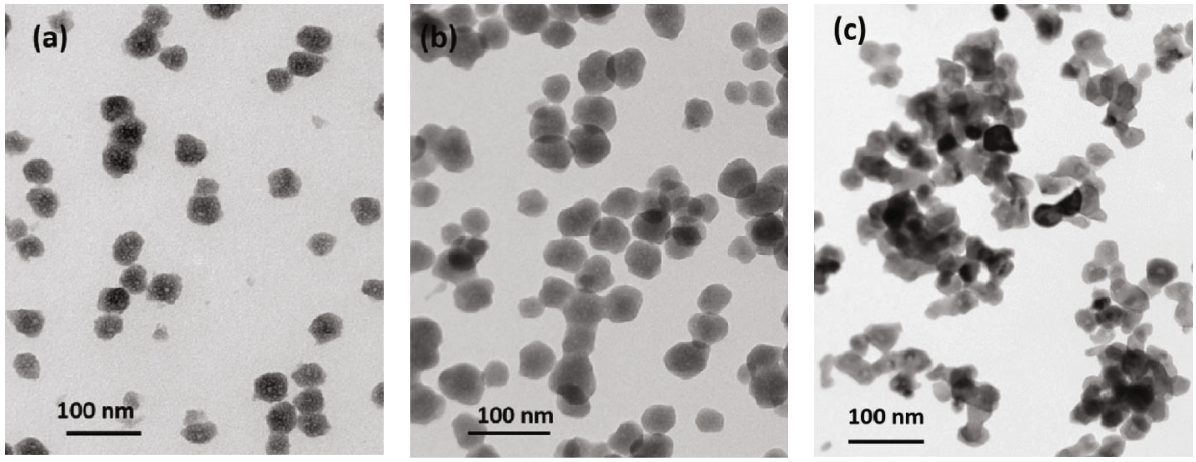

(a) (b) (c)

FIGURE 2: TEM images of (a) the precursor of the core NPs ($Y(OH)CO_3$:12% Er^{3+}), (b) the precursor of the core-shell NPs (Y_2O_3:Er^{3+}@$Y(OH)CO_3$:Yb^{3+}, Ho^{3+}), and (c) the final products of Y_2O_2S: Er^{3+}@Y_2O_2S:Yb^{3+},Ho^{3+} NPs.

Ho^3+ were obtained as shown in Figure 2(b). It can be observed that the NPs remain the spherical shape with an enlarged mean particle size of ≈55 nm. This increase of the particle size after the shell coating indicates the formation of the core-shell structure [21, 22]. The final products of Y_2O_2S: Er^{3+} @Y_2O_2S: Yb^3+, Ho^{3+} were obtained after the sulfidation process at a high temperature of 800°C, as shown in Figure 2(c). It can be seen that the particles aggregate together after calcination. These agglomerating particles make it challenging to obtain an accurate statics particle size distribution.

The core-shell Y_2O_2S:Er^{3+}@Y_2O_2S:Yb^{3+},Ho^{3+} UC NPs exhibit bright UCL of green color, while the Yb^{3+}, Er^{3+}, Ho^{3+} triple-doped Y_2O_2S NPs show red emission color. As shown in Figure 3, both samples present the green UC emission in the range of 516-570 nm and red ones at 623-698 nm. Compared with the spectrum of Y_2O_2S:Yb^{3+},Ho^{3+} sample, the visible emissions of the core-shell sample centered at 545, 655 and 750 nm, correspond to the $^5S_2$, $^5F_4 \rightarrow {}^5I_8$, $^5F_5 \rightarrow {}^5I_8$ and $^5S_2$, $^5F_4 \rightarrow {}^5I_7$ transitions of Ho^{3+} ions, respectively [1]. Similarly, compared with the Y_2O_2S:Yb^{3+},Er^{3+} NPs, the green emissions of the core-shell sample centered at 540 and 555 nm contribute from the $^2H_{11/2} \rightarrow {}^4I_{15/2}$ and $^4S_{3/2} \rightarrow {}^4I_{15/2}$ transitions of Er^{3+} ions, respectively. And the red emission at ≈ 675 nm is resulted from the $^4F_{9/2} \rightarrow {}^4I_{15/2}$ transition of Er^{3+} ions [23, 24]. The measured quantum yield of Y_2O_2S:Er^{3+}@Y_2O_2S:Yb^{3+},Ho^{3+} UC NPs is about 0.45%.

Although the UCL from the Ho^{3+} and Er^{3+} ions are realized in both samples of Y_2O_2S:Yb^{3+},Er^{3+},Ho^{3+} and core-shell Y_2O_2S:Er^{3+} @Y_2O_2S:Yb^{3+},Ho^{3+}, the green emissions from Ho^{3+} ions are significantly enhanced in the core-shell sample. While the red UCL from Er^{3+} ions is dominant in the Y_2O_2S:Yb^{3+},Er^{3+},Ho^{3+} sample. The intensity ratios (I) of green (G) to red (R) emissions (I_G/I_R) of Y_2O_2S:Er^{3+} @ Y_2O_2S:Yb^{3+}, Ho^{3+} and Y_2O_2S:Yb^{3+}, Er^{3+}, Ho^{3+} samples are are 2.8 and 0.3, respectively. This is due to the cross relaxation between Er^{3+} and Ho^{3+} ions in the Y_2O_2S:Yb^{3+}, Er^{3+},Ho^{3+} sample, which suppresses the emission of Ho^{3+} and enhances the red emission simultaneously. However, in the core-shell sample of Y_2O_2S:Er^{3+}@Y_2O_2S:$Yb^{3+}$$Ho^{3+}$, the cross relaxation between Er^{3+} and Ho^{3+} ions is effectively suppressed by constructing the core-shell structure where Er^{3+} is in the core and Ho^{3+} is in the shell. Therefore, the core-shell sample exhibits dominant green emissions from Ho^{3+} ions, yet the conventional triple-ion doped sample present red UCL from Er^{3+} ions.

The possible UCL processes of Y_2O_2S:Er^{3+}@Y_2O_2S:Yb^{3+}, Ho^{3+} sample under 980 nm excitation are shown in Figure 4. The UCL of Ho^{3+}, Yb^{3+} ions present green, red and weak NIR emissions. Firstly, the sensitizer of Yb^{3+} ion is excited to the $^2F_{5/2}$ energy level after absorbing the 980 nm photon via ground state absorption (GSA) process. Then the Ho^{3+} ion is excited to the high levels of $^5S_2$ and $^5F_4$ via continuous energy transfer (ET) processes of ET1 and ET2 from Yb^{3+} ion (process (1) and process (2) in Figure 4). The excited Ho^{3+} ion at levels of $^5S_2$ and $^5F_4$ generates green emission through $^5S_2$, $^5F_4 \rightarrow {}^5I_8$ transition, and a small portion of them decays to the intermediate state of $^5I_7$ via $^5S_2$, $^5F_4 \rightarrow {}^5I_7$ to exhibit weak NIR emission [1]. This process of NIR emission will populate the $^5I_7$ level. In addition, the cross relaxation (CR) processes of $^5S_2$, $^5F_4$ (Ho^{3+}) + $^5I_8$ (Ho^{3+}) → $^5I_4$ (Ho^{3+}) + $^5I_7$ (Ho^{3+}) (CR1) and $^5I_4$(Ho^{3+}) + $^5I_8$ (Ho^{3+}) → $^5I_6$ (Ho^{3+}) + $^5I_7$ (Ho^{3+}) (CR2) may occur and further populate the energy level of $^5I_7$. Then Ho^{3+} ions at the state of $^5I_7$ will be pumped to the high excited state of $^5I_5$ after absorbing the 980 nm photon, and then emit red UCL through the $^5I_5 \rightarrow {}^5I_8$ transition.

In terms of the UCL processes of Yb^{3+}, Er^{3+} ions, the Yb^{3+} is firstly pumped to the excited level of $^2F_{5/2}$ by absorbing a 980 photon, and then return to the ground state by transferring the energy to an Er^{3+} ion in the core via ET3 and ET5, as shown in Figure 4. These ET processes will excite the Er^{3+} from ground state of $^4I_{15/2}$ to the high level of $^4F_{7/2}$ through $^4I_{11/2}$ level. The Er^{3+} ion at $^4F_{7/2}$ then decays to the $^2H_{11/2}$, and $^4S_{3/2}$ levels via non-radiative relaxation, producing green emission through $^2H_{11/2} \rightarrow {}^4I_{15/2}$, and $^4S_{3/2} \rightarrow {}^4I_{15/2}$ transitions [6, 7]. The excited Er^{3+} ion at $^4I_{11/2}$ level can also decay to the $^4I_{13/2}$ state,

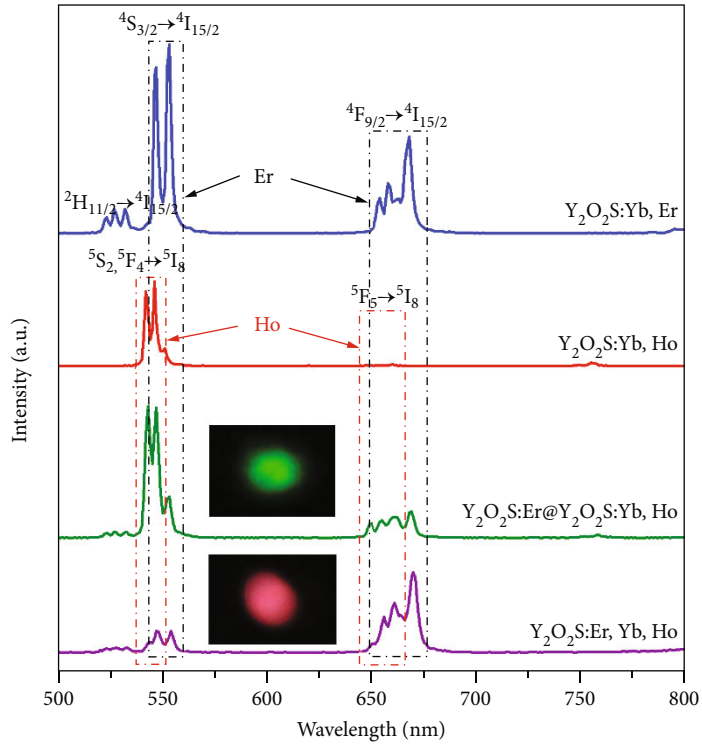

FIGURE 3: Up-conversion emission spectra of Y_2O_2S: Yb^{3+}, Er^{3+}, Y_2O_2S: Yb^{3+}, Ho^{3+}, Y_2O_2S: Er^{3+} @ Y_2O_2S: Yb^{3+}, Ho^{3+} and Y_2O_2S: Yb^{3+}, Er^{3+}, Ho^{3+} samples under 980 nm excitation.

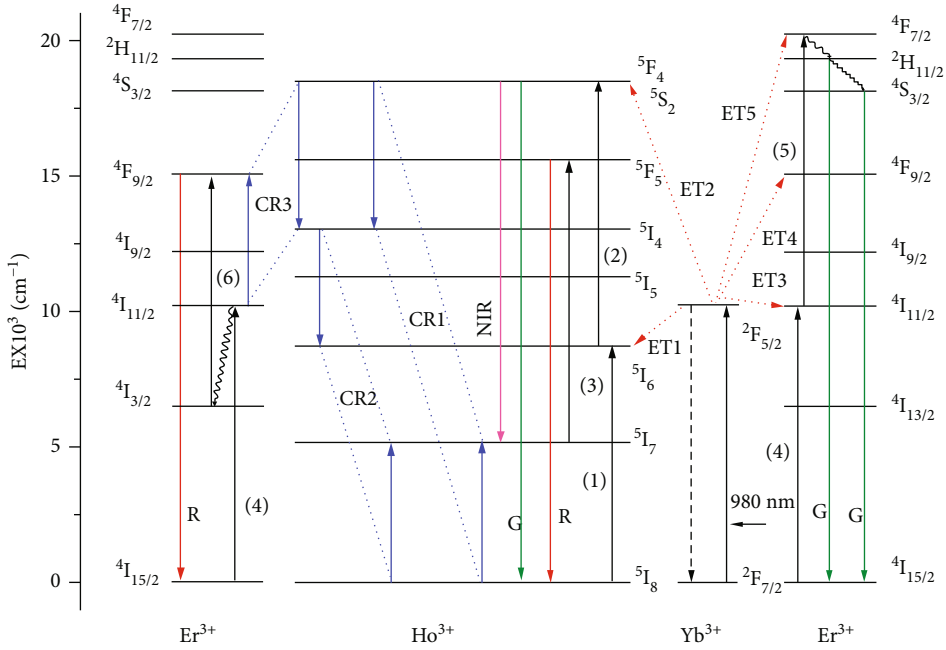

FIGURE 4: The UCL processes of Y_2O_2S: Er^{3+} @ Y_2O_2S: Yb^{3+}, Ho^{3+} and Y_2O_2S: Yb^{3+}, Er^{3+}, Ho^{3+} samples under 980 nm excitation.

and then populate to the $^4F_{9/2}$ by absorbing a 980 photon. Then the red emission from Er^3+ ion occurs via transition of $^4F_{9/2} \rightarrow {}^4I_{15/2}$.

Notably, due to the small distance between the Er^{3+} and Ho^{3+} ions in the Y_2O_2S: Yb^{3+}, Er^{3+}, Ho^{3+} sample, the cross relaxations of $^5S_2$, $^5F_4$ (Ho^{3+}) + $^4I_{11/2}$ (Er^{3+}) $\rightarrow$ $^5I_4$ (Ho^{3+}) + $^4F_{9/2}$ (Er^{3+}) (CR3) can easily occur in the conventional triple-ion doped sample. This CR3 process significantly increases the population of Er^{3+} ion at the $^4F_{9/2}$ level, which results in the much stronger red emission (due to

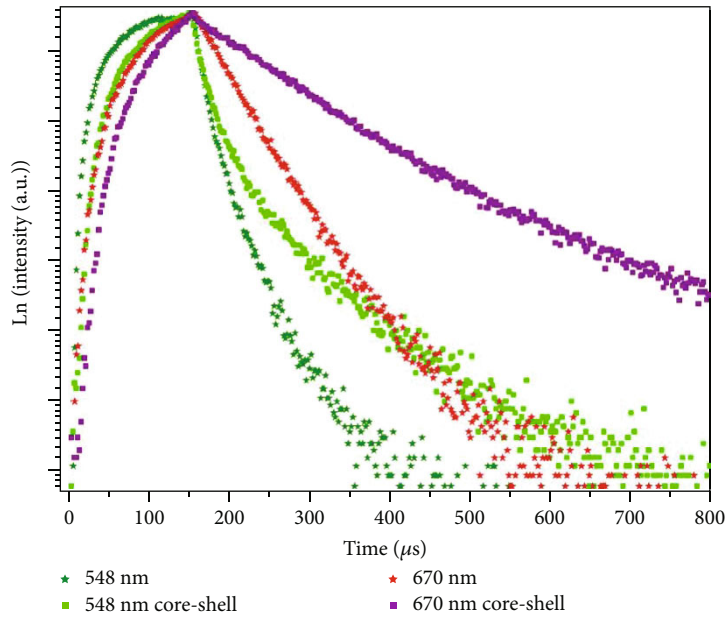

Figure 5: Fluorescence decay curves of red (670 nm) and green (548 nm) emissions of Y_2O_2S: Er^{3+} @ Y_2O_2S: Yb^{3+}, Ho^{3+} (Core-Shell) and Y_2O_2S: Yb^{3+}, Er^{3+} samples under 980 nm excitation.

Table 1: Calculated luminescence lifetimes of Y_2O_2S: Er^{3+} @ Y_2O_2S: Yb^{3+}, Ho^{3+} and Y_2O_2S: Yb^{3+}, Er^{3+} samples.

Transition	Lifetime (μs)	
	Y_2O_2S: Er^{3+} @ Y_2O_2S: Yb^{3+}, Ho^{3+}	Y_2O_2S: Yb^{3+}, Er^{3+}
$^4S_{3/2} \rightarrow {}^4I_{15/2}$ (548 nm)	37.8	21.8
$^4F_{9/2} \rightarrow {}^4I_{15/2}$ (670 nm)	139.1	46.1

$^4F_{9/2} \rightarrow {}^4I_{15/2}$) in the Y_2O_2S: Yb^{3+}, Er^{3+}, Ho^{3+} sample than that of the core-shell Y_2O_2S: Er^{3+} @ Y_2O_2S: Yb^{3+}, Ho^{3+} sample. Meanwhile, this CR3 process also decreases the population of Ho^{3+} ion at the $^5S_2$, $^5F_4$ states, thereby, suppressing the green emission in the Y_2O_2S: Yb^{3+}, Er^{3+}, Ho^{3+} sample. The different UCL and ET processes in the Y_2O_2S: Yb^{3+}, Er^{3+}, Ho^{3+} and core-shell Y_2O_2S: Er^{3+} @ Y_2O_2S: Yb^{3+}, Ho^{3+} samples indicate the formation of the core-shell structure and provide a possible route for adjustment of emission color.

Further, the fluorescence decay curves of Y_2O_2S: Er^{3+} @ Y_2O_2S: Yb^{3+}, Ho^{3+} (Core-Shell) and Y_2O_2S: Yb^{3+}, Er^{3+} samples were measured as shown in Figure 5. All the decay curves present non-exponential profile due to the relaxation and energy transfer processes between the Yb^{3+} ions and Er^{3+}, Ho^{3+} ions. According to the lifetime equation of $\tau = \int_0^\infty I(t)\,tdt / \int_0^\infty I(t)dt$, where τ is the calculated luminescence lifetime and I(t) is the luminescence intensity at time after the cutoff of the excitation light, the calculated lifetimes of green and red emissions of Y_2O_2S: Yb^{3+}, Er^{3+} and Y_2O_2S: Er^{3+} @ Y_2O_2S: Yb^{3+}, Ho^{3+} samples are listed in Table 1. It shows that lifetimes of red and green emissions of the core-shell Y_2O_2S: Er^{3+} @ Y_2O_2S: Yb^{3+}, Ho^{3+} sample are much longer than that of the Y_2O_2S: Yb^{3+}, Er^{3+} sample. This is owing to the effective protection of the shell layer for the emissions of Er^{3+} ions in the core. In addition, due to the non-radiative relaxation of $^4I_{11/2} \rightarrow {}^4I_{13/2}$ in the red emission process, the rising time of the red emission at 670 nm is much longer than that of the green emission at 548 nm. Therefore, the fluorescence decay measurements support the luminescence mechanisms.

4. Conclusion

The Y_2O_2S:Er^{3+}@Y_2O_2S:Yb^{3+}, Ho^{3+} core-shell NPs are synthesized by the homogeneous co-precipitation method combining with the solid-gas sulfidation route. Investigations on the UCL show that the emissions from Er^{3+} and Ho^{3+} ions are achieved simultaneously in the core-shell NPs. This is due to the efficient energy transfers of $Yb^{3+} \rightarrow Ho^{3+}$ within the shell layer and $Yb^{3+} \rightarrow Er^{3+}$ between the shell and the core. However, the core-shell Y_2O_2S: Er^{3+} @ Y_2O_2S: Yb^{3+}, Ho^{3+} and the triple-ion doped Y_2O_2S: Yb^{3+}, Er^{3+}, Ho^{3+} samples present mainly green emission from Ho^{3+} ions ($I_G/I_R = 2.8$) and red luminescence from Er^{3+} ions ($I_G/I_R = 0.3$), respectively. The reason is that the cross relaxation between Er^{3+} and Ho^{3+} ions can easily occur due to the small distance between them in the Y_2O_2S: Yb^{3+}, Er^{3+}, Ho^{3+} sample. While on the other hand, this cross relaxation can be successfully suppressed by the core-shell structure where Ho^{3+} is in the shell and Er^{3+} is in the core. Therefore, the unique core-shell Y_2O_2S nanostructure could offer new channels for energy transfers and presents novel UC luminescence properties.

Data Availability

The data used to support the findings of this study are included within the article.

Conflicts of Interest

There is no conflict of interest regarding the publication of this paper.

Acknowledgments

The authors thank the National Natural Science Foundation of China (11504039), Fundamental Research Funds for the Central Universities (Grant No. 017192610, 017192617) for their financial support.

Supplementary Materials

The supplementary material provides the experiments on the optimum rare earth doping concentrations and the particle size distribution of the precursors of the core and core-shell nanoparticles. *(Supplementary Materials)*

References

[1] W. Xu, H. Zhao, Y. Li, L. Zheng, Z. Zhang, and W. Cao, "Optical temperature sensing through the upconversion luminescence from Ho3+/Yb3+ codoped CaWO4," *Sensors and Actuators B*, vol. 188, no. 11, pp. 1096–1100, 2013.

[2] G. Y. Chen, H. Ågren, T. Y. Ohulchanskyy, and P. N. Prasad, "Light upconverting core–shell nanostructures: nanophotonic control for emerging applications," *Chemical Society Reviews*, vol. 44, no. 6, pp. 1680–1713, 2015.

[3] Y. H. Zhang, L. X. Zhang, R. R. Deng et al., "Multicolor barcoding in a single upconversion crystal," *Journal of the American Chemical Society*, vol. 136, no. 13, pp. 4893–4896, 2014.

[4] G. W. Wang, H. F. Zou, H. G. Zhang et al., "Preparation and luminescence properties of novel 3D $Lu_2O_2S:Eu^{3+}$ microstructures," *Materials Letters*, vol. 128, pp. 256–258, 2014.

[5] X. L. Zhou, M. M. Xing, T. Jiang et al., "Afterglow performance enhancement and mechanism studies on Y2O2S:Eu,Mg,Ti prepared via cold isostatic pressing," *Journal of Alloys and Compounds*, vol. 585, pp. 376–383, 2014.

[6] G. A. Kumar, M. Pokhrel, A. Martinez, R. C. Dennis, I. L. Villegas, and D. K. Sardar, "Synthesis and spectroscopy of color tunable Y2O2S:Yb3+,Er3+ phosphors with intense emission," *Journal of Alloys and Compounds*, vol. 513, pp. 559–565, 2012.

[7] Y. Tian, Y. Fu, M. Xing, and X. Luo, "Upconversion luminescence properties of Y_2O_3:Yb, Er and Y_2O_2S:Yb, Er nanoparticles prepared by complex precipitation," *Journal of Nanomaterials*, vol. 2015, Article ID 573253, 7 pages, 2015.

[8] M. Pokhrel, G. A. Kumar, C. G. Ma et al., "Electronic and optical properties of Er-doped Y_2O_2S phosphors," *Journal of Materials Chemistry C*, vol. 3, no. 43, pp. 11486–11496, 2015.

[9] S. W. Kim, T. Hasegawa, T. S. Abe et al., "Abnormal improvement in emission of lanthanum oxysulfide phosphor La 2 O 2 S:Tb 3+ synthesized by a novel method, thermal decomposition in eutectic molten salt," *Ceramics International*, vol. 42, no. 8, pp. 10389–10392, 2016.

[10] M. Mikami and A. Oshiyama, "First-principles band-structure calculation of yttrium oxysulfide," *Physical Review B*, vol. 57, no. 15, pp. 8939–8944, 1998.

[11] L. Han, M. M. Pan, Y. Lv et al., "Fabrication of $Y_2O_2S:Eu^{3+}$ hollow nanofibers by sulfurization of $Y_2O_3:Eu^{3+}$ hollow nanofibers," *Journal of Materials Science: Materials in Electronics*, vol. 26, no. 2, pp. 677–684, 2015.

[12] T. Hirai and T. Orikoshi, "Preparation of yttrium oxysulfide phosphor nanoparticles with infrared-to-green and -blue upconversion emission using an emulsion liquid membrane system," *Journal of Colloid and Interface Science*, vol. 273, no. 2, pp. 470–477, 2004.

[13] M. M. Xing, W. H. Cao, T. Pang, and X. Q. Ling, "Synthesis of monodisperse spherical Y_2O_2S:Yb,ho upconversion nanoparticles," *Solid State Communications*, vol. 149, no. 23-24, pp. 911–914, 2009.

[14] X. X. Luo and W. H. Cao, "Upconversion luminescence of holmium and ytterbium co-doped yttrium oxysulfide phosphor," *Materials Letters*, vol. 61, no. 17, pp. 3696–3700, 2007.

[15] R. Martín-Rodríguez, S. Fischer, A. Ivaturi et al., "Highly efficient IR to NIR upconversion in $Gd_2O_2S:Er^{3+}$ for photovoltaic applications," *Chemistry of Materials*, vol. 25, no. 9, pp. 1912–1921, 2013.

[16] F. Wang and X. Liu, "Upconversion Multicolor Fine-Tuning: Visible to Near-Infrared Emission from Lanthanide-Doped NaYF4Nanoparticles," *Journal of the American Chemical Society*, vol. 130, no. 17, pp. 5642-5643, 2008.

[17] C. Zhang and J. Y. Lee, "Prevalence of anisotropic Shell growth in rare earth Core–Shell Upconversion nanocrystals," *ACS Nano*, vol. 7, no. 5, pp. 4393–4402, 2013.

[18] H. S. Qian and Y. Zhang, "Synthesis of hexagonal-phase core –shell $NaYF_4$ nanocrystals with tunable upconversion fluorescence," *Langmuir*, vol. 24, no. 21, pp. 12123–12125, 2008.

[19] T. Pang, W. Cao, M. Xing, W. Feng, S. Xu, and X. Luo, "Preparation and upconversion luminescence of monodisperse Y_2O_2S:Yb/ho-silica/aminosilane core-shell nanoparticles," *Journal of Rare Earths*, vol. 28, no. 4, pp. 509–512, 2010.

[20] F. Vetrone, R. Naccache, V. Mahalingam, C. G. Morgan, and J. A. Capobianco, "The active-core /active-shell approach: a strategy to enhance the upconversion luminescence in lanthanide-doped nanoparticles," *Advanced Functional Materials*, vol. 19, no. 18, pp. 2924–2929, 2009.

[21] N. J. J. Johnson and F. C. J. M. van Veggel, "Sodium lanthanide fluoride core–shell nanocrystals: a general perspective on epitaxial shell growth," *Nano Research*, vol. 6, no. 8, pp. 547–561, 2013.

[22] G.-s. Yi and G.-M. Chow, "Water-soluble NaYF4:Yb,Er(tm)/NaYF4/polymer Core/Shell/Shell nanoparticles with significant enhancement of Upconversion fluorescence," *Chemistry of Materials*, vol. 19, no. 3, pp. 341–343, 2007.

[23] K. A. Gonçalves, J. F. S. Bitencourt, J. C. R. Mittani, and S. H. Tatumi, "Study of radiation induced effects in the luminescence of nanostructured Al2O3: Yb, Er crystals," *IOP Conference Series: Materials Science and Engineering*, vol. 15, 2010.

[24] X. Yin, H. Wang, Y. Tian, M. Xing, Y. Fu, and X. Luo, "Three primary color emissions from single multilayered nanocrystals," *Nanoscale*, vol. 10, no. 20, pp. 9673–9678, 2018.


The Scientific
World Journal
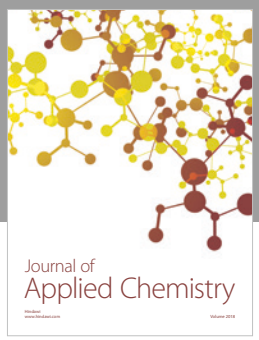
Journal of
Applied Chemistry
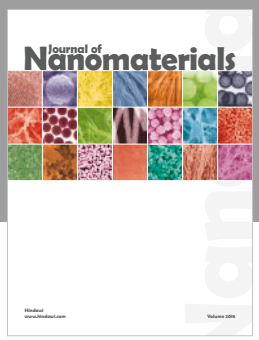
Journal of
Nanomaterials

Scientifica

International Journal of
Polymer Science
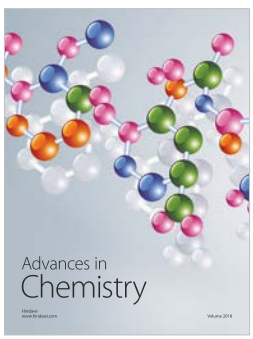
Advances in
Chemistry

Hindawi
Submit your manuscripts at
www.hindawi.com
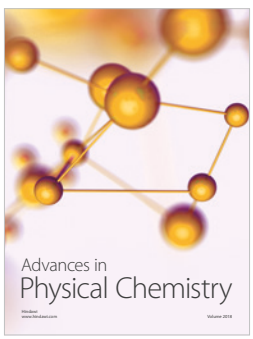
Advances in
Physical Chemistry

International Journal of
Analytical Chemistry
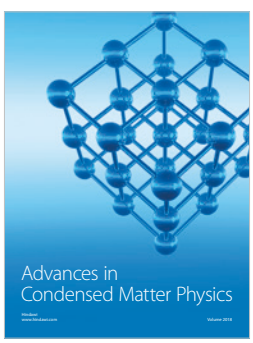
Advances in
Condensed Matter Physics
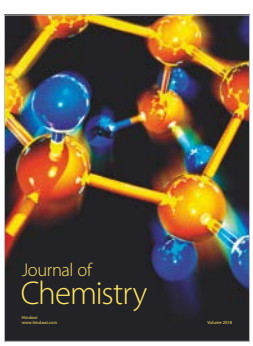
Journal of
Chemistry

International Journal of
Biomaterials
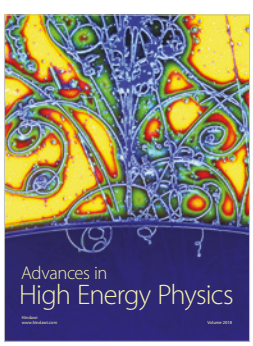
Advances in
High Energy Physics

Journal of
Engineering

Journal of
Nanotechnology

International Journal of
Corrosion

Journal of
Materials

BioMed
Research International
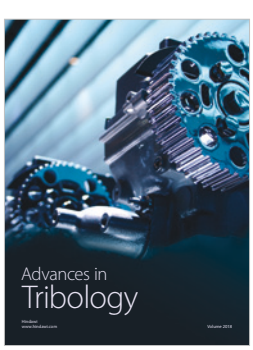
Advances in
Tribology
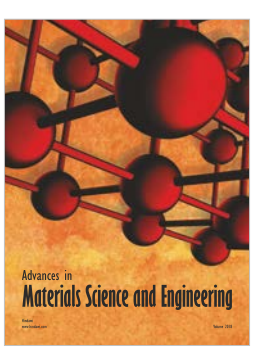
Advances in
Materials Science and Engineering